Acta Crystallographica Section D
Biological Crystallography
ISSN 0907-4449

Structure of macrophomate synthase

Toyoyuki Ose,[a] Kenji Watanabe,[b] Min Yao,[a] Mamoru Honma,[b] Hideaki Oikawa[c] and Isao Tanaka[a]*

[a]Division of Biological Sciences, Graduate School of Science, Hokkaido University, Sapporo 060-0810, Japan, [b]Division of Applied Bioscience, Graduate School of Agriculture, Hokkaido University, Sapporo 060-8589, Japan, and [c]Division of Chemistry, Graduate School of Science, Hokkaido University, Sapporo 060-0810, Japan

Correspondence e-mail: tanaka@castor.sci.hokudai.ac.jp

Received 11 March 2004
Accepted 14 April 2004

PDB Reference:
M. commelinae MPS, 1izc, r1izcsf.

Macrophomate synthase (MPS) is an enzyme that catalyzes an extraordinarily complex conversion reaction, including two decarboxylations, two carbon–carbon bond formations and a dehydration, to form the benzoate analogue macrophomate from a 2-pyrone derivative and oxalacetate. Of these reactions, the two carbon–carbon bond formations are especially noteworthy because previous experiments have indicated that they proceed *via* a Diels–Alder reaction, one of the most widely used reactions in organic synthesis. The structural evidence that MPS catalyzes an intermolecular Diels–Alder reaction has been reported recently [Ose *et al.* (2003), *Nature (London)*, **422**, 185–189]. Interestingly, the tertiary structure as well as the quaternary structure of MPS are similar to those of 2-dehydro-3-deoxygalactarate (DDG) aldolase, a carbon–carbon bond-forming enzyme that catalyzes the reversible reaction of aldol condensation/cleavage. Here, the structure of MPS is described in detail and compared with that of DDG aldolase. Both enzymes have a $(\beta/\alpha)_8$-barrel fold and are classified as belonging to the enolase superfamily based on their reaction strategy. The basic principles for carbon–carbon bond formation used by both MPS and DDG aldolase are the same with regard to trapping the enolate substrate and inducing subsequent reaction. The major differences in the active sites between these two enzymes are the recognition mechanisms of the second substrates, 2-pyrone and DDG, respectively.

1. Introduction

Only a few enzymes that catalyze different types of multistep chemical conversion reactions have been discovered to date. For example, the crystal structure of dehydroquinate synthase revealed that this enzyme catalyzes consecutive chemical reactions in a single active site (Bender *et al.*, 1989). Recently, we reported the crystal structure of macrophomate synthase (MPS; Ose *et al.*, 2003). This enzyme catalyzes extraordinarily complex chemical transformations from oxalacetate and 2-pyrone (1) (Fig. 1*a*) to macrophomate (2) (Fig. 1*a*) (Oikawa *et al.*, 1999; Watanabe, Mie *et al.*, 2000*a*,*b*). The first reaction catalyzed by MPS is the decarboxylation of oxalacetate. The pyruvate enolate produced is expelled as pyruvate from the active site after a proton addition (route *a*). However, if a second 2-pyrone substrate such as compounds (2) and (4) is present, procedure of the Diels–Alder reaction has been proposed (Watanabe, Mie *et al.*, 2000*a*). The Diels–Alder reaction first gives bicyclic adducts (5), which are degraded into the benzoate anologues macrophomates, such as (1) and (3). Therefore, at least three chemical reactions are involved in the reaction pathway of MPS.

The Diels–Alder reaction is a cycloaddition in which an alkene (dienophile) adds to a 1,3-diene to form a six-membered ring; its mechanism involves the overlap of the π-orbitals of the two unsaturated systems. In nature, the Diels–Alder reaction has been thought to occur concomitantly with many other chemical transformations. Since there are many expected natural Diels–Alder adducts, mechanistic study of natural Diels–Alderases is of great interest (Ichihara & Oikawa, 1998, 1999). The search for a natural Diels–Alderase in a biosynthesis pathway has long been in progress. Natural Diels–Alderases such as solanapyrone synthase (Katayama *et al.*, 1998; Oikawa *et al.*, 1995, 1998), lovastatin nonaketide synthase (Auclair *et al.*, 2000; Kennedy *et al.*, 1999) and macrophomate synthase (MPS; Watanabe, Mie *et al.*, 2000*a*) have been reported in the biosynthesis of secondary metabolite products. However, the details of catalysis by natural Diels–Alderases are poorly understood.

Artificial enzymes that can catalyze the Diels–Alder reaction have been generated using biomolecules such as RNA (Frauendorf & Jäschke, 1998) and protein antibodies (Braisted & Schultz, 1991; Gouverneur *et al.*, 1993; Hilvert *et al.*, 1989; Ylikauhaluoma *et al.*, 1995). The reactions catalyzed by these biomolecules show remarkable enantioselectivity and diastereoselectivity. A detailed mechanism of Diels–Alderase antibodies has been proposed on the basis of X-ray crystallography and molecular orbital calculations (Heine *et al.*, 1998; Romesberg *et al.*, 1998; Xu *et al.*, 1999).

We determined the crystal structure of MPS from the phytopathogenic fungus *Macrophoma commelinae*, isolated from spots on the leaves of the tsuyukusa plant *Commelina communis*, at 1.7 Å resolution (Ose *et al.*, 2003). In the report, we describe the enzymatic strategies that promote the Diels–Alder reaction based on the crystal structure and on kinetic analysis of the mutants. The active site of MPS reveals several ingenious features for catalyzing the Diels–Alder reaction, including the existence of residues that make catalytically important hydrogen bonds to the 2-pyrone. In the present paper, we describe additional structural details and discuss the reactions catalyzed by this protein.

No other enzyme has been given the annotation MPS. Furthermore, the sequence of MPS showed no significant similarity to known proteins in a homology search using the *BLAST* program (Altschul *et al.*, 1990), although 2-dehydro-3-deoxygalactarate (DDG) aldolase and 4-hydroxy-2-oxovalerate aldolase showed weak similarity. Crystal structures of DDG aldolase (Izard & Blackwell, 2000) are available (PDB codes 1dxe and 1dxf). DDG aldolase catalyzes the reversible reaction of DDG to pyruvate and tartronic semialdehyde (Fig. 1*b*). The crystal structures of both MPS and DDG aldolase formed a $(\beta/\alpha)_8$-barrel (or TIM-like barrel) with distinctive C-terminal α-helices that are swapped

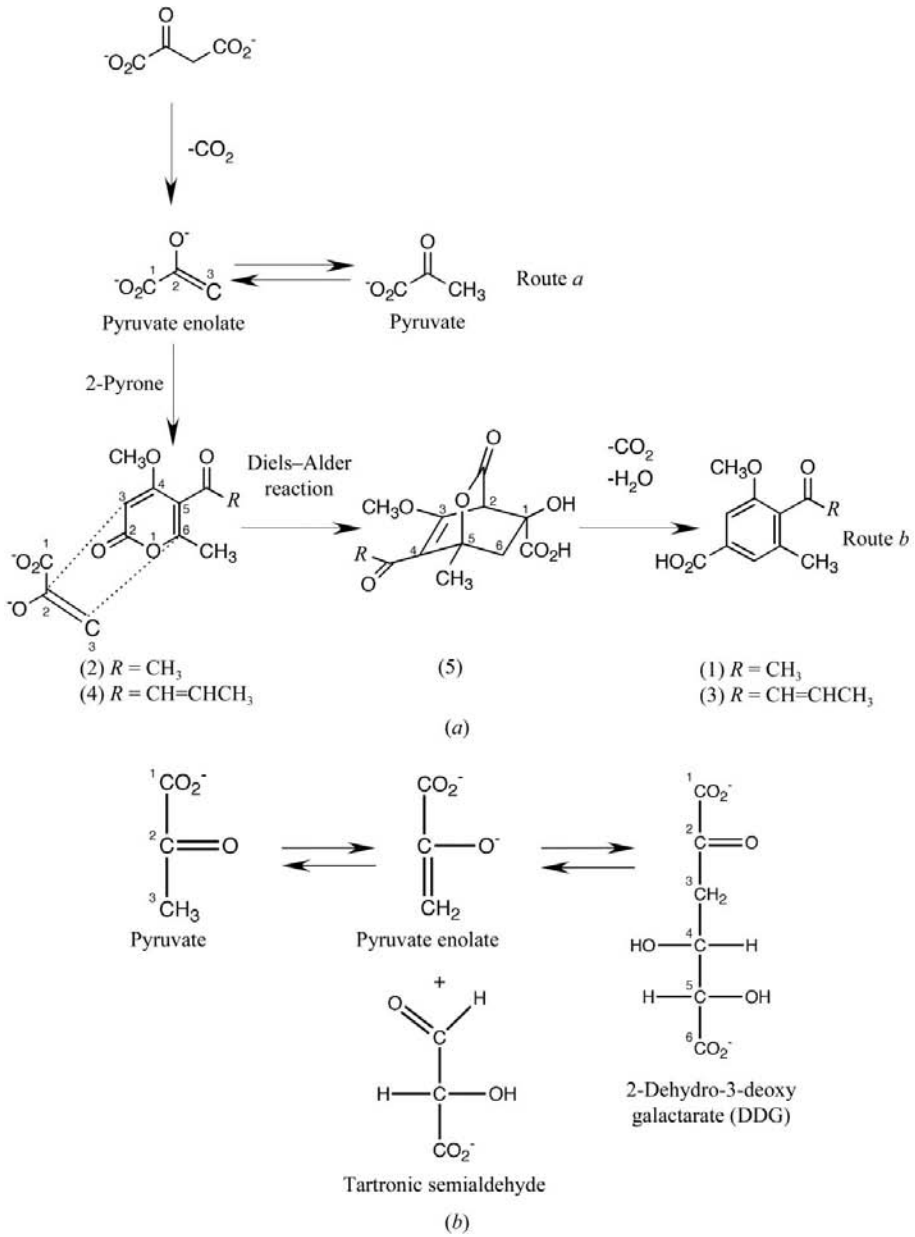

Figure 1
Enzymatic reactions catalyzed by MPS and DDG aldolase. (*a*) Total reaction scheme of MPS. Route *a*, decarboxylation without 2-pyrone. Route *b*, multi-step transformation with 2-pyrone. Macrophomate (1) and 2-pyrone (2) were discovered in *M. commelinae*. MPS also can convert pyrenocin A (4) into pyrenocheatic acid A (3), which are phytotoxins from onion pink rot. (*b*) Enzymatic reactions catalyzed by DDG aldolase. Both enzymes have a specific strategy to produce the reactive enolate.

Table 1
Data statistics.

Values in parentheses are for the highest resolution shell.

		SeMet		
Crystal	Native	Peak	Edge	Remote
Crystallographic data				
Beamline	PF BL18B	PF BL18B		
Space group	$P6_322$	$R32$		
Wavelength (Å)	1.0000	0.9795	0.9797	0.9803
Resolution (Å)	1.70 (1.79–1.70)	2.30 (2.42–2.30)	2.30 (2.42–2.30)	2.30 (2.42–2.30)
No. reflections				
Observed	266163 (17767)	128483 (11322)	141293 (20517)	141050 (20583)
Unique	41139 (3901)	12358 (1690)	12509 (1805)	12487 (1803)
Completeness (%)	91.3 (61.0)	99.1 (94.5)	100.0 (100.0)	100.0 (100.0)
Average redundancy	6.5 (4.5)	10.4 (6.7)	11.3 (11.4)	11.3 (11.4)
Average $I/\sigma(I)$	6.5 (2.5)	8.2 (4.6)	7.7 (3.7)	7.8 (3.6)
$R_{\rm merge}$†	0.08 (0.31)	0.08 (0.19)	0.09 (0.22)	0.087 (0.23)
$R_{\rm lambda}$‡	—	0.028	0.031	—
Phasing				
Phasing power§				
Iso	—	0.544	0.776	-
Ano	—	3.782	3.098	1.203
$R_{\rm Cullis\_iso}$¶	—	0.71	0.61	-
Overall figure of merit††	—		0.568	
Refinement				
Resolution (Å)	20–1.70			
Total No. non-H atoms				
Protein	2271			
Others	273			
Solvent	266			
R factor‡‡	0.1811			
$R_{\rm free}$ factor§§	0.2040			
R.m.s.d. bond lengths (Å)	0.008			
R.m.s.d. bond angles (°)	1.417			
Average B factor (Å^2)	18.58			
Ramachandran analysis¶¶ (%)				
Most favoured	90.2			
Additionally allowed	9.4			
Generously allowed	0.4			

† $R_{\rm meas} = \sum_h [m(m-1)]^{1/2} \sum_j |\langle I\rangle_h - I_{h,j}| / \sum_h \sum_j I_{h,j}$, where $\langle I\rangle_h$ is the mean intensity of symmetry-equivalent reflections and m is the redundancy. ‡ $R_{\rm lambda} = \sum \big||F_{\lambda j}| - |F_{\lambda 0}|\big| / \sum |F_{\lambda 0}|$, where $F_{\lambda j}$ is the structure factor of the data collected at λ_j and $F_{\lambda 0}$ is the structure factor of the data collected at 0.9803 Å. § Phasing power = $\langle|F_H(\text{calc})|\rangle / \langle$phase-integrated lack of closure$\rangle$. ¶ $R_{\rm Cullis}$ = $\langle$phase-integrated lack of closure$\rangle / \langle|F_{PH} - F_P|\rangle$. †† Figure of merit after the initial phasing using the program *SHARP* (de La Fortelle & Bricogne, 1997). ‡‡ R factor = $\sum |F_{\rm obs} - F_{\rm calc}| / \sum F_{\rm obs}$, where $F_{\rm obs}$ and $F_{\rm calc}$ are the observed and calculated structure-factor amplitudes. §§ The $R_{\rm free}$ factor was calculated as for the R factor, using a random 10% subset of all reflections. ¶¶ The Ramachandran plot was calculated using *PROCHECK* (Laskowski *et al.*, 1993).

between two monomers. Significantly, the structures around the active sites as well as the architecture of the oligomerization are common to the two enzymes. A comparison of the reaction mechanisms of these two molecules based on the tertiary structure is also described in the present paper.

2. Experimental procedues

2.1. Purification and crystallization

Macrophomate synthase was purified from the *Escherchia coli* overproducing strain BL21 harbouring the gene that encodes macrophomate synthase from *M. commelinae*, as described previously (Watanabe, Oikawa *et al.*, 2000). Selenomethionyl recombinant MPS for multiwavelength anomalous diffraction (MAD) phasing was expressed in methionine-auxotroph *E. coli* B834 (DE3) cells (Stratagene) transformed with pET-30b(+)/MPS plasmid. The fraction containing MPS was pooled and dialyzed against 50 m*M* piperazine-1,4-bis(2-ethanesulfonic acid) (PIPES) pH 7.0 and concentrated by ultrafiltration using CentriPlus-30 and Centricon-30 microconcentrators (Amicon Inc.) to a final concentration of 10 mg ml^{-1}. The protein concentrations of the enzyme preparations were determined either by measuring the absorbance at 280 nm or by using a protein assay kit (Bio-Rad) with bovine immunoglobulin G as a standard. The purity of the protein was analyzed by MALDI–TOF mass spectrometry (Voyager DE-PRO, PerSeptive Biosystems) and by enzyme specific activity assay. Macrophomate synthase activity assay was analyzed by reverse-phase HPLC following previously described procedures (Watanabe, Mie *et al.*, 2000*c*). All the crystallization experiments were carried out using the hanging-drop vapour-diffusion method in a 24-well Linbro tissue-culture plates (ICN Inc.) at 291 K. Each drop was formed by mixing equal volumes (2 ± 0.5 µl) of protein solution and reservoir solution. The protein concentration was 10 mg ml^{-1} prior to mixing with the reservoir solution. The initial attempts at crystallization were carried out using Hampton Research Crystal Screens I and II and AS, MPD, PEG and PEG–LiCl Grid Screens.

The first crystals were grown using condition No. C4 of the Hampton Research PEG 6000 Grid Screen [0.1 *M* Tris pH 7.0, 20.0%(*w*/*v*) PEG 6000]. The crystals diffracted to 6 Å or better. This condition was further optimized by varying the pH, protein concentration, temperature, precipitants and additives. After the initial crystallization trial using screening kits, we prepared a protein solution containing 5.0 m*M* $MgCl_2$ with 50 m*M* PIPES buffer pH 7.0, 10%(*v*/*v*) 2-propanol for further optimization of crystallization conditions such as pH, protein concentration, temperature, precipitants and additives.

2.2. Data collection

The diffraction measurements were carried out at beamline BL18B of the Photon Factory (PF), Tsukuba, Japan using a

CCD detector (Quantum 4R). All X-ray diffraction data sets were recorded from crystals flash-cooled to 100 K after soaking for about 10 s in mother liquor containing 15% glycerol. An X-ray absorption spectrum of an Se-MPS crystal was collected around the Se *K* absorption edge by measuring the fluorescence signal perpendicular to the beam during a wavelength scanning performed at BL18B. All data were processed with *MOSFLM* (Leslie, 1993) and the *CCP*4 suite (Collaborative Computational Project, Number 4, 1994).

Native crystals suitable for X-ray diffraction experiments were obtained using the following conditions: 23% polyethylene glycol 3350 (PEG 3350) in the presence of 10% 2-propanol as an additive with 100 m*M* PIPES–KOH. The crystal shape was basaltiform, with a diameter and length of 100 and 600 µm, respectively. This crystal enabled us to collect a native data set to 1.70 Å resolution. The crystal belongs to space group $P6_322$ (form *A*), with unit-cell parameters $a = b = 106.7$, $c = 120.8$ Å. The asymmetric unit contains one molecule of MPS, corresponding to a V_M value (Matthews, 1968) of 2.92 Å^3 Da^{-1} and a solvent content of 57.5%.

SeMet-substituted MPS was also crystallized for use in the multiple-wavelength anomalous diffraction method (MAD) following the previously described method with slight modifications. The best crystallization condition for Se-MPS was the same as that for native crystals except for the use of a slightly lower concentration of the precipitant PEG 3350 (20%). Two kinds of Se-MPS crystals were obtained. SeMet form *A* crystals diffracted to 2.3 Å and belonged to space group *R*32, with unit-cell parameters $a = b = 122.6$, $c = 95.8$ Å. The asymmetric unit contains two molecules, corresponding to a V_M value of 2.09 Å^3 Da^{-1} and a solvent content of 40.6%. Form *B* SeMet crystals, belonging to space group *R*32 with unit-cell parameters $a = b = 121.5$, $c = 199.8$ Å, diffracted poorly and the reflection data were only used to 3.2 Å resolution. The asymmetric unit contains two molecules, corresponding to a V_M value of 2.09 Å^3 Da^{-1} and a solvent content of 40.6%. The *c* unit-cell parameter is about twice as long as that the type *A* Se-MPS crystals. The data-collection and processing statistics are shown in Table 1.

2.3. Structure determination and refinement

The MAD data were further scaled using the *CCP*4 program suite. Of 11 Se-atom sites, four were initially

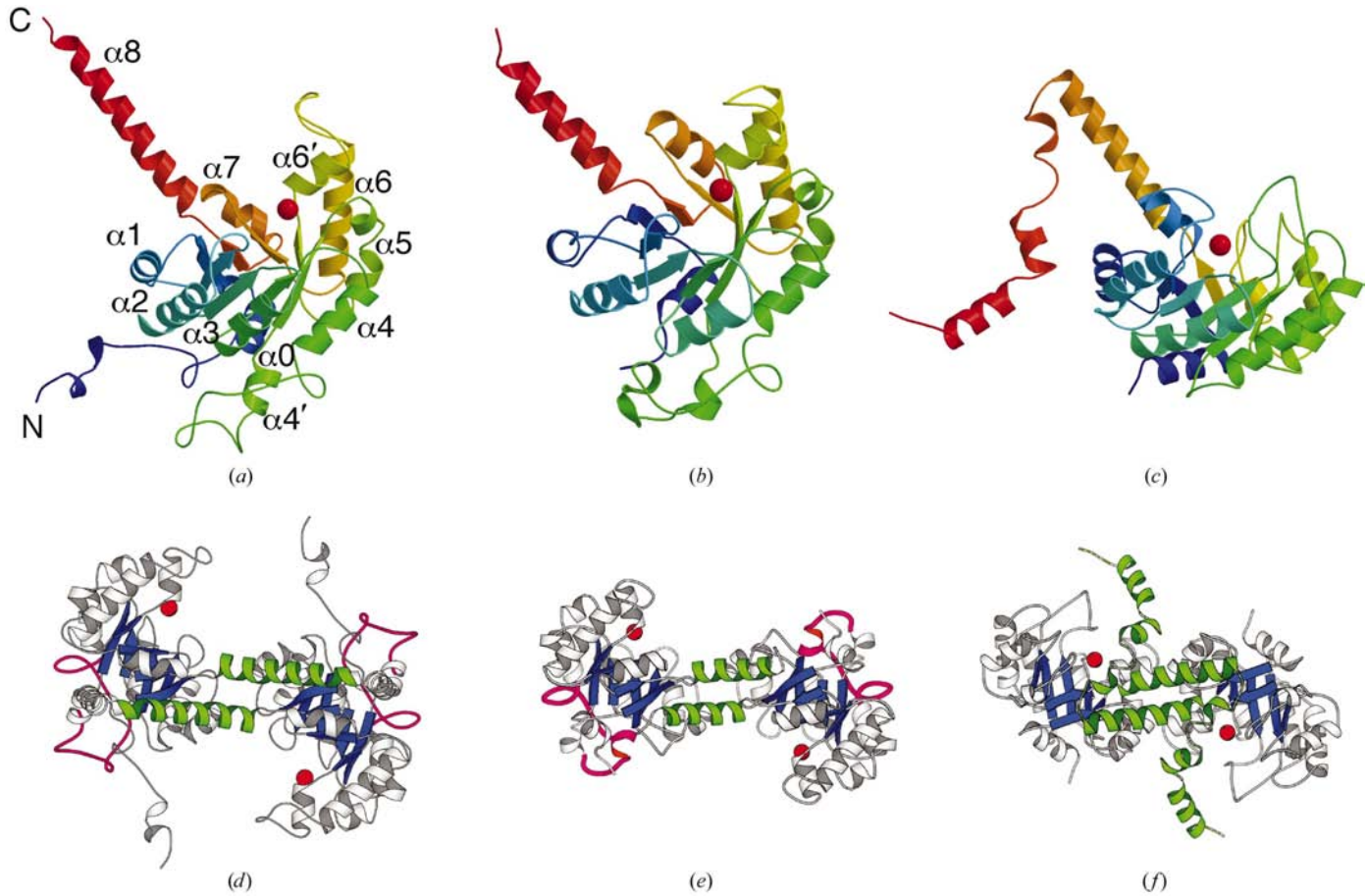

Figure 2
Monomeric and dimeric structures of MPS (*a*, *d*), DDG aldolase (Izard & Blackwell, 2000) (*b*, *e*) and phosphoenolpyruvate mutase (Huang *et al.*, 1999) (*c*, *f*). The protomer models (*a*, *b*, *c*) are coloured according to sequence by a rainbow colour ramp from blue at the N-terminus to red at the C-terminus of the monomers. The three enzymes have long helices in the C-terminal regions that are utilized to form a swapping dimer related by the twofold axis (*d*, *e*, *f*). The divalent magnesium ion (red sphere) is located in the C-terminal region of the β-barrel. MPS and DDG aldolase have long loops (coloured in magenta) that cover the active sites of neighbouring protomers related by the threefold axis.

located using the program *SOLVE* (Terwilliger & Berendzen, 1999). After the initial experimental phases had been calculated from these four selenium sites, seven additional sites were found by the difference Fourier method using *SHARP* (de La Fortelle & Bricogne, 1997). A model including 299 out of 339 residues was built manually using the program *O* (Jones *et al.*, 1991) from a density map that had been re-phased with all 11 Se-atom sites and modified with solvent flattening by the program *SHARP*/*SOLOMON* (Abrahams & Leslie, 1996) at 2.3 Å resolution. After several rounds of molecular-dynamics refinement using the program *CNS* (Brünger *et al.*, 1998) using the MAD data, with manual fitting using the program *O*, the model was transferred to the native crystal by molecular replacement using the program *AMoRe* (Navaza, 1994).

The molecular-dynamics refinement was performed using the program *CNS* with 20.0–1.7 Å resolution native data and 10% of the data were selected for calculation of the $R_{\rm free}$ factor in order to monitor refinement. A pyruvate molecule and a magnesium ion were located from the $\sigma_{\rm A}$-weighted $2F_{\rm o} - F_{\rm c}$ and $F_{\rm o} - F_{\rm c}$ maps and were used in the last few rounds of refinement. Their topology and parameter files were obtained from the HIC-up site (Kleywegt & Jones, 1998). The final structure of the MPS–pyruvate complex, which consists of 299 residues, one magnesium ion, one pyruvate molecule and 360 water molecules, was refined to an $R_{\rm free}$ of 20.3% and an R factor of 17.6% with a root-mean-square deviation of 0.008 Å in bond length and 1.37° in bond angles. This model was checked using the program *PROCHECK* (Laskowski *et al.*, 1993). Of the 299 resides in the model, 90.1% are in the most favoured regions and 9.4% are in additional allowed regions (one residue is in a generously allowed region) in the Ramachandran plot. One N-terminal and 40 C-terminal residues cannot be modelled because of their flexibility. The statistics of structural refinement are shown in Table 1.

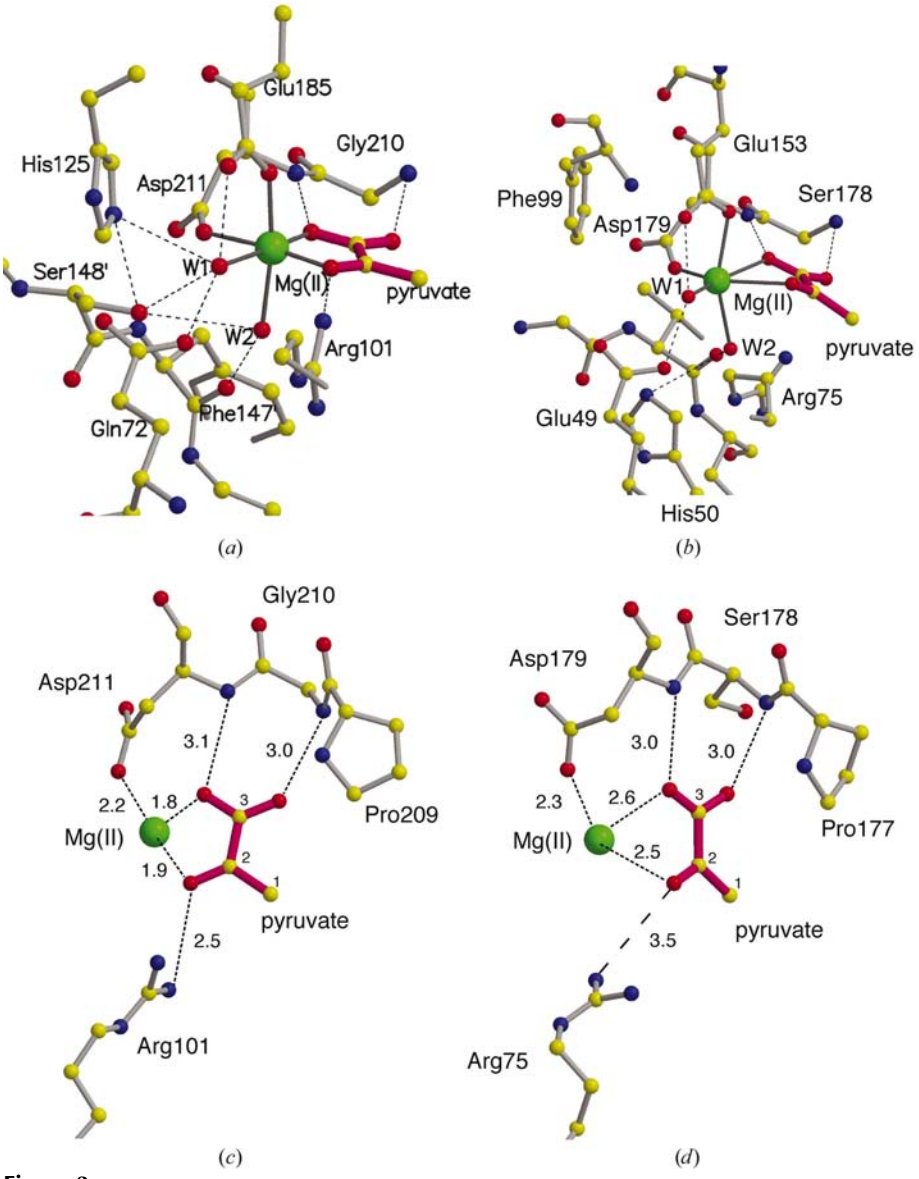

Figure 3
Active-site comparison of MPS (*a*, *c*) and DDG aldolase (*b*, *d*). Both enzymes are viewed from almost the same direction. Octahedrally coordinated magnesium ions and their ligands are shown. The ligands are the carboxyl O atoms of Glu and Asp, the C2 carbonyl and C1 carboxyl O atoms of pyruvate (magenta) and two water molecules, W1 and W2. The dotted lines indicate interactions *via* hydrogen bonding. The atoms are coloured as follows: red, oxygen, blue, nitrogen, yellow, carbon and green, magnesium.

3. Results

3.1. The molecular arrangement

Three different MPS crystals have been analyzed. The crystals of the native type with space group $P6_322$ diffracted to 1.7 Å resolution. The other two forms are SeMet MPS forms *A* and *B*, both of which belong to space group *R*32; they have *c* axes of quite different lengths. There is one molecule in the asymmetric unit of the native and SeMet form *A* crystals. The structures of MPS from these crystals are hexameric, with crystallographic point-group symmetry 32 (Ose *et al.*, 2003). In contrast, in SeMet form *B* crystals the twofold symmetry is non-crystallographic. The protomer core region consists of an eight-stranded β-barrel surrounded by 8 + 3 α-helices with a $(\beta/\alpha)_8$-barrel (triosephosphate isomerase-like barrel) fold. The connectivity of the barrel is $\alpha0'$–$\beta1$–$\alpha1$–$\beta2$–$\alpha2$–$\beta3$–$\alpha3$–$\beta4$–$\alpha4$–$\alpha4'$–$\beta5$–$\alpha5$–$\beta6$–$\alpha6'$–$\alpha6$–$\beta7$–$\alpha7$–$\beta8$–$\alpha8$ (Fig. 2*a*). The three additional α-helices that do not belong to the $(\beta/\alpha)_8$-barrel are indi-

cated with a prime. Interestingly, the C-terminal α8 helix (residues 275–298) of each protomer protrudes from the core and joins the β/α-barrel core of the twofold-related protomer (Fig. 2*d*). This long helix plays a role in forming a dimer (crystallographic symmetry in native and SeMet form *A* and non-crystallographic symmetry in SeMet form *B*) by providing ionic as well as hydrophobic forces and takes part to complete the $(\beta/\alpha)_8$-barrel fold in another protomer. The dimers assemble to make up a hexameric unit with a threefold crystallographic rotation axis in all three crystal forms. The buried surface area and the number of residues between protomers show that inter-subunit interactions of the dimer are stronger than inter-dimer interactions.

The arrangement of forming a swapped dimer with a $(\beta/\alpha)_8$-barrel has been observed in the structures of phosphoenolpyruvate mutase (Figs. 2*c* and 2*f*; Huang *et al.*, 1999) and DDG aldolase (Figs. 2*b* and 2*e*; Izard & Blackwell, 2000). DDG aldolase forms a hexamer with the same assembly as that of MPS. Phosphoenolpyruvate mutase assembles into a tetramer with point-group symmetry 222. A *DALI* structural similarity search (Holm & Sander, 1993) and an *EMBL-SSM* (secondary-structure matching) search revealed that MPS is most similar to DDG aldolase, one of the class II aldolases (PDB code 1dxe; *Z* score 26.9; r.m.s.d. 2.2 Å for 247 C_α atoms with *DALI*). The class II aldolases are metal-containing enzymes in which the substrate is coordinated to a divalent metal cation such as magnesium.

The SCOP protein-structure database (Murzin *et al.*, 1995) currently distinguishes 25 superfamilies of $(\beta/\alpha)_8$-barrel fold enzymes, where the members of a superfamily have a probable common evolutionary origin. Enzymes containing $(\beta/\alpha)_8$-barrels show a particularly wide range of functions; DDG aldolase belongs to the phosphoenolpyruvate/pyruvate-domain type based on its structure, whereas it is classified as type II aldolase by reaction type. The precursor of MPS is presumably an oxalacetate decarboxylase that generate a pyruvate enolate, which is expelled as pyruvate from the active site. Its additional function as a Diels–Alderase may have been acquired accidentally *a posteriori*. After proton abstraction, pyruvate can become a substrate (pyruvate enolate) for a Diels–Alder-type cycloaddition reaction. The two enzymes share an enolase superfamily from the view of having of a reaction strategy that involves divalent metal-ion-assisted enolization of the substrate carboxylate anion. Obtaining structural and reaction information on the two enzymes allows us to understand the evolutionary modification of using a common structural motif to catalyze different overall reactions.

3.2. The active site

A previous study showed that MPS requires Mg^{2+} ion as a divalent metal-ion cofactor in order to express macrophomate synthesis activity or oxalacetate decarboxylation activity (Watanabe, Mie *et al.*, 2000*a*). The activity is inhibited by 3 m*M* EDTA and recovered by adding Mg^{2+}. The K_d value for Mg^{2+} is 9.9×10^{-8} *M*. These findings show that MPS recognizes Mg^{2+} specifically. There is one MPS active site per monomer, which is at the C-terminal end of the β-barrel covered by the loop from the threefold-related chain. The Mg^{2+} ion was recognized as a 5σ peak in the $F_o - F_c$ map (Ose *et al.*, 2003) with an octahedral coordination (Fig. 3*a*). The geometry around the Mg^{2+} ion is nearly ideal. The two coordination sites of the magnesium ion are occupied by the side chains of Glu185 (2.1 Å) and Asp211 (2.2 Å). Glu185 is positioned in the C-terminal loop of β-strand β5 and Asp211 is

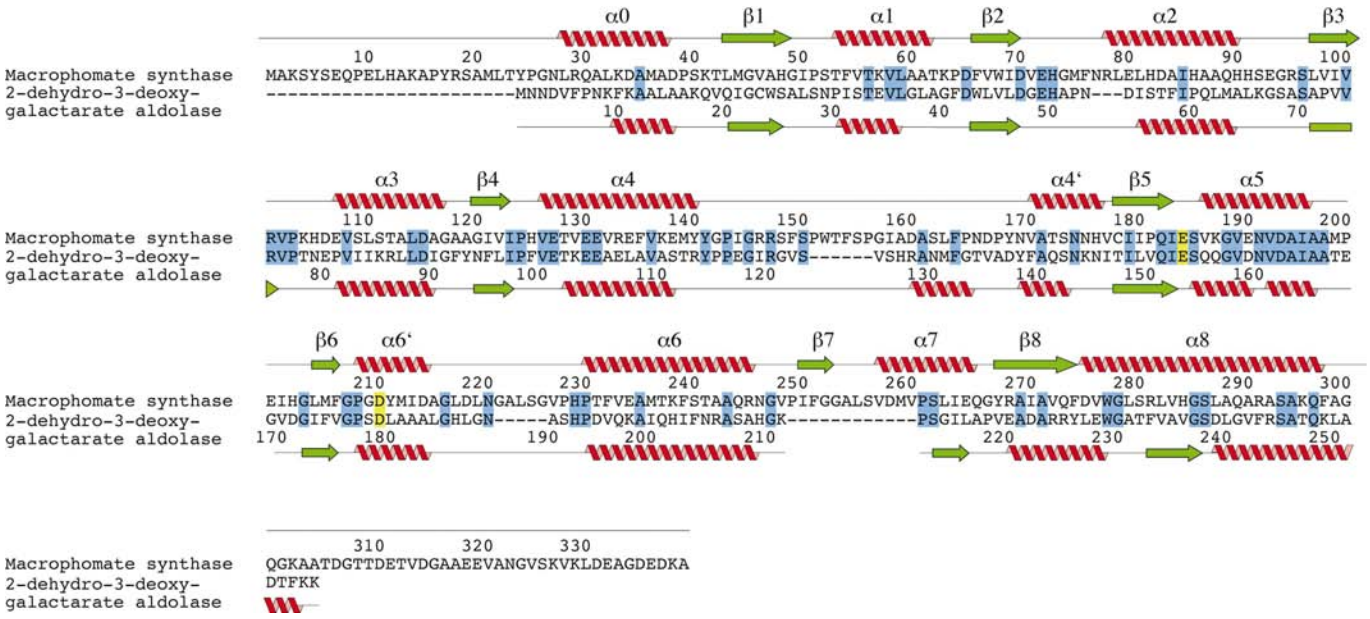

Figure 4
Secondary structure of MPS and DDG aldolase from *E. coli* shown along with the amino-acid sequence alignment. α-Helices and β-strands are coloured red and green, respectively. The residues that coordinate divalent magnesium ion are emphasized in yellow. The residues highlighted in light blue represent complete conservation.

located in the α-helix α6 (Fig. 4). The two additional coordination sites of the Mg^{2+} ion are filled with two water molecules, W1 (2.3 Å) and W2 (2.3 Å), which are in turn hydrogen-bonded to the protein. W1 is hydrogen bonded to the side-chain carboxyl O atom of Glu72 (2.6 Å), the side-chain N atom of His125 (3.2 Å), the side-chain carboxyl O atom of Glu185 (2.7 Å) and the side-chain hydroxyl O atom of Ser148′ (3.3 Å) from the protomer related by the threefold axis. W2 is bonded to the side-chain hydroxyl O atom of Ser148′ (3.4 Å) and the main-chain carbonyl O atom of Phe149′ (2.4 Å), both of which are from the protomer related by the threefold axis. The last two coordination sites of the magnesium ion are occupied by the C2 carbonyl (1.9 Å) and C1 carboxyl (1.8 Å) O atoms of pyruvate.

Pyruvate is the product of the first step of the decarboxylation reaction as well as the substrate of the second step, [4 + 2] cycloaddition with 2-pyrone. Therefore, knowing the position and configuration of pyruvate is critically important for the investigation of both reactions. The high-resolution electron-density map enabled us to define the precise orientation of the bound pyruvate (Fig. 3*c*), two carboxyl O atoms of which are also hydrogen bonded to the main-chain amide protons of Gly210 (3.0 Å) and Asp211 (3.1 Å). This complex is further stabilized by interaction between the carbonyl O atom of pyruvate and the side chains of Arg101 (2.5 Å). The fact that the active site is positioned at the interface of a threefold-related protomer may play a role in catalytic efficiency. The structure of the contacting loop varies slightly between the three crystal packings; it therefore follows that the loop region is flexible.

3.3. Structure comparison with DDG aldolase

MPS shows sequence similarity to DDG aldolase (about 20% identity), whereas it does not show any significant sequence similarity to phosphoenolpyruvate mutase. Thus, the following comparison is mainly with DDG aldolase. The crystal structure of DDG aldolase has been reported at 1.8 Å resolution (Izard & Blackwell, 2000). Secondary-structural elements of MPS and DDG aldolase as defined by *PROCHECK* (Laskowski *et al.*, 1993) are given in Fig. 4 with a sequence alignment. The sequence alignment shows that the two proteins correspond well. The active sites of these proteins are both located at the C-terminal end of the β-barrel core (Fig. 2). The Mg^{2+} ions that are essential to catalysis can be recognized in both structures and are coordinated by two carboxylate side chains from residues Glu185 (Glu153) and Asp211 (Asp178) (Figs. 3*a* and 3*b*); the residue numbers for DDG aldolase are indicated in parentheses. These two residues, which are positioned on the same loop and helix, are conserved in the sequence alignment. Superimposition of the monomeric structures of these two proteins shows that the core $(\beta/\alpha)_8$-barrel structures and protruding C-terminal helices are highly conserved. Some differences can be seen in the loop regions such as the N-terminus and the middle part (residues 140–170 in MPS), which are in contact with the protomer related by the threefold rotation axis (Fig. 5). The C-terminal helix of MPS is composed of 23 residues (residues 276–298) and is longer than that of DDG aldolase (15 residues, 240–254). These long helices play an important role in interacting with the twofold-related protomer. Therefore, MPS is more tightly associated in the hexameric assembly than DDG aldolase. These small differences result in molecular surface areas that are not alike. The protomer molecular surface area of MPS is 15 160 $Å^2$, while the surface area of DDG aldolase is 11 573 Å. The total buried surface areas on dimerization are 3812 and 2958 $Å^2$ and on trimerization are 2507 and 1958 $Å^2$ for MPS and DDG aldolase, respectively. Molecular surfaces were calculated using *CNS* (Brünger *et al.*, 1998) with a 1.4 Å probe radius.

Pyruvate is also recognized in the structure of DDG aldolase, as shown in Fig. 3(*d*). The recognition mechanism of the pyruvate is the same as that in MPS: Ser209 and Asp210 in MPS correspond to Ser178 and Asp179 in DDG aldolase, respectively. The distances from the carboxylate O atoms of pyruvate to these amide N atoms are about 3.0 Å. Interestingly, the side chains of the second residues of both enzymes (Asp210 and Asp179) are also coordinated to Mg^{2+}. These regions are in the middle part of the α-helices. The C2 carbonyl and C1 carboxyl O atoms of pyruvate also interact with Mg^{2+} in both enzymes. The other coordination sites are also common to the two enzymes. They are glutamate and two water molecules (W1 and W2) (Figs. 3*a* and 3*b*). However, the following interactions observed in MPS are not found in DDG aldolase: W1 and His125, W1 and Ser148′, and the C1 carbonyl O atom of pyruvate and Arg101 (Fig. 3). As is the case in the MPS reaction, pyruvate is

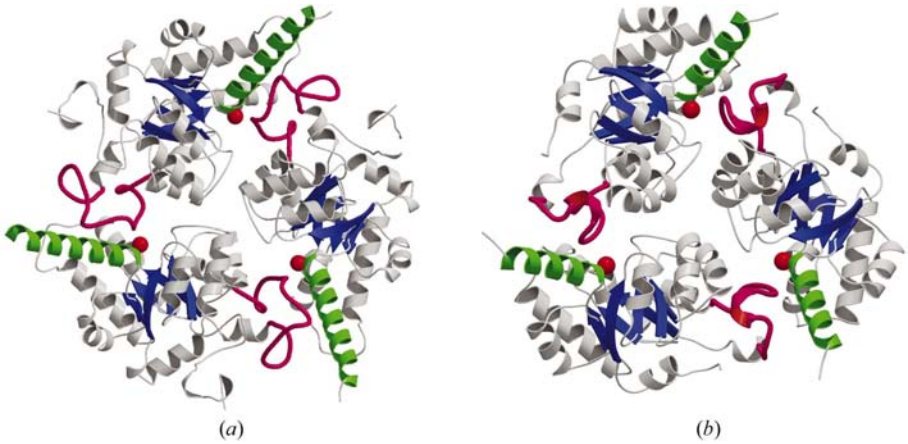

Figure 5
Comparison of the trimeric structures of MPS (*a*) and DDG aldolase (*b*) related by a crystallographic threefold axis. Each flexible loop coloured in magenta (there are helical parts in this region of DDG aldolase) is joined to the active site of the next protomer. The C-terminal long α-helices (green) and core β-barrels (blue) are also highlighted, along with the magnesium ion (red).

one of the substrates for the next condensation reaction of DDG aldolase. Although oxalate is structurally similar to pyruvate, it is recognized in a different manner in the active site of phosphoenolpyruvate mutase (Huang *et al.*, 1999).

The guanidinium N atom of Arg101 is about 2.5 Å from the C2 carbonyl O atom of pyruvate in MPS, whereas the distance from corresponding Arg75 is about 3.5 Å in the DDG aldolase structure. The octahedral coordination is somewhat less than ideal in DDG aldolase. These differences may explain the different affinities of the two enzymes for Mg^{2+}. Divalent ions such as Co^{2+} or Mn^{2+} can replace Mg^{2+} in the DDG aldolase reaction, while the enzymatic activity of MPS can be detected only with Mg^{2+} and not with other divalent cations. Arg75 is important in the abstraction of an α-proton from pyruvate by reducing the pK_a of the phosphate ion that interacts with the side chain of Arg75 in the DDG aldolase reaction (Izard & Blackwell, 2000). Arg101 forms critical hydrogen bonding with 2-pyrone that reduces the lowest unoccupied molecular orbital (LUMO) energy for the Diels–Alder reaction in MPS (Ose *et al.*, 2003).

The least-squares superposition of MPS and DDG aldolase around the active sites shows that both the positions and the residue types are conserved, for example Glu72/Glu49 (MPS/DDG aldolase), Arg101/Arg75, Glu185/Glu153, Pro209/Pro177 and Asp211/Asp179. A comparison of the active sites shows that a subtle difference in the coordination causes catalytic differences. $(\beta/\alpha)_8$-barrel fold proteins are found to make up approximately 10% of enzymes (Gerlt & Babbitt, 1998) and can exhibit a wide range of functions. The functional diversity of the $(\beta/\alpha)_8$-barrel enzymes can be achieved by these local changes or modifications.

4. Discussion and conclusions

DDG aldolase catalyzes the reversible aldol cleavage–condensation reaction of 2-dehydro-3-deoxygalactarate to pyruvate and tartronic semialdehyde, while MPS catalyzes a conversion from oxalacetate and 2-pyrone (2) to macrophomate (1) (Fig. 1*a*). Thus, the catalytic activities of these two enzymes differ significantly.

DDG aldolase catalyzes a one-step condensation reaction. In contrast, our previous experiments showed that the conversion reaction of MPS is an extraordinarily complex chemical transformation involving decarboxylations, carbon–carbon bond formations and dehydration (Watanabe, Mie *et al.*, 2000*a*). We are now at the stage of examining these conversion reactions based on the atomic resolution structure of MPS. Here, we present the details of the enzymatic reaction of MPS along with some comparison to the reaction of DDG aldolase. The detailed orientation of the bound pyruvate allows us to visualize the whole reaction process that occurs in the two enzymes. The MPS reaction proceeds *via* three steps.

The first step of the MPS reaction is the decarboxylation of the oxalacetate. The decarboxylation mechanism of this enzyme is the same as that of the metal-dependent oxalacetate decarboxylases from *Pseudomonas putida* (Waldrop *et al.*, 1994) or *Acetobacter xylinum* (Benziman *et al.*, 1978) described previously (Piccirilli *et al.*, 1987; Steinberger & Westheimer, 1949). Owing to the Lewis acidity of the magnesium, the decarboxylation occurs to form the enolate anion, which is stabilized by an electron sink provided from the divalent cation (Piccirilli *et al.*, 1987). The incorporated oxalacetate should form a similar chelation complex to that of pyruvate (Figs. 3*a* and 6). In this complex structure, the peptide chain containing Phe207, Gly208 and Pro209 forces the C4 carboxylate underneath the chelated plane of the oxalacetate. This model is consistent with the stereochemical course of the decarboxylation predicted by a previous experiment with (3*S*)-[3-^{2}H]-oxalacetate (Watanabe, Mie *et al.*, 2000*a*).

DDG aldolase first catalyzes the enolization of pyruvate and this enzyme-bound enolate then attacks the polarized

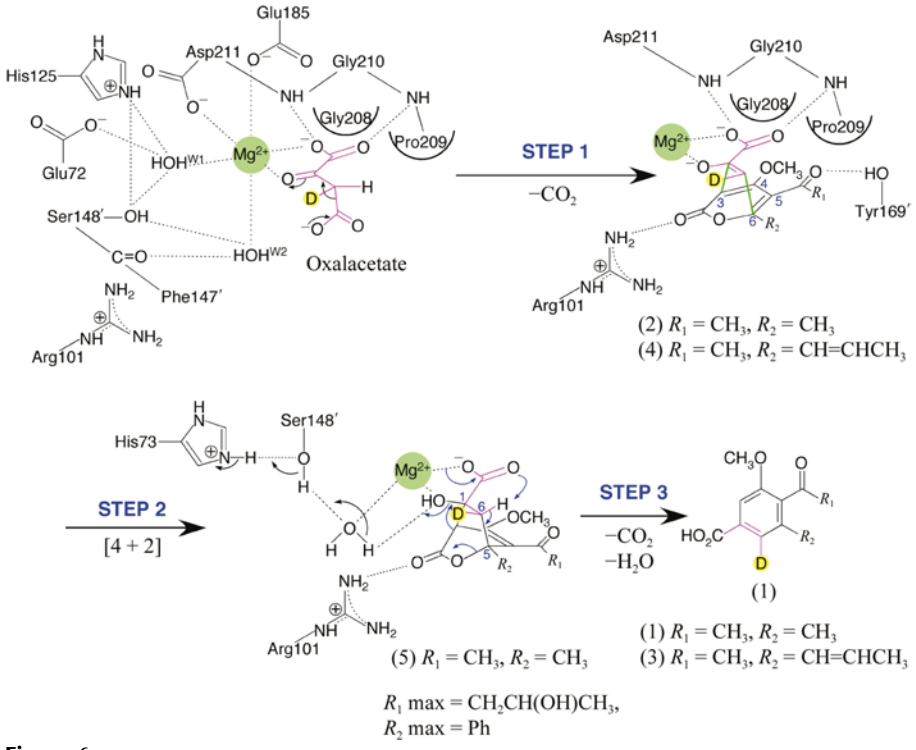

Figure 6
Proposed reaction mechanism of oxalacetate decarboxylation, Diels–Alder reaction and concomitant reorganization. Charged and hydrogen-bonding interactions are shown as dotted lines and the residues involved in the hydrophobic interactions are indicated with arcs. The carbon skeleton of the oxalacetate is shown in purple. The green lines represent the carbon–carbon bonds formed by the Diels–Alder reaction. The bulkiest substituants permitted at the R_1 and R_2 positions of substrates are 2-hydroxylpropyl and phenyl groups, respectively, as shown in the figure.

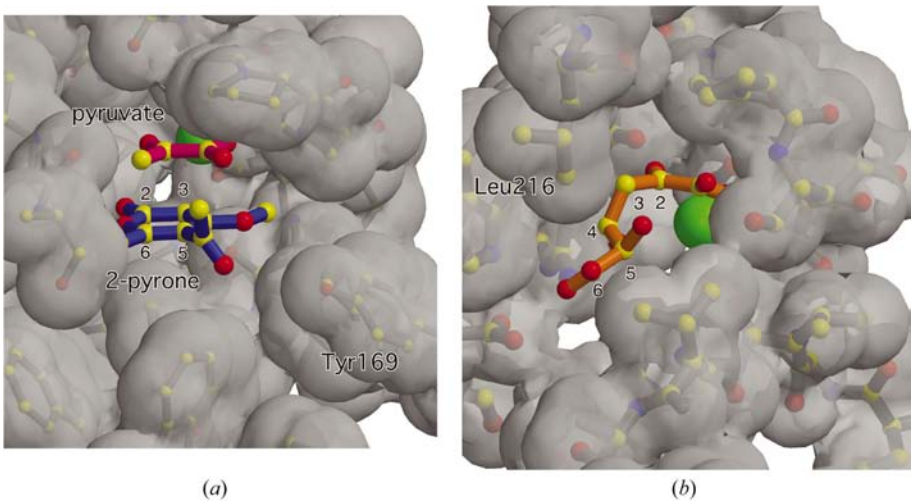

Figure 7
Space-filling models around the active site complexed (*a*) with pyruvate and modelled 2-pyrone (in MPS) and (*b*) with DDG (in DDG aldolase). Pyruvate is colored magenta and 2-pyrone blue; DDG is coloured orange. The atoms of both figures are coloured as follows: red, oxygen; blue, nitrogen; yellow, carbon; green, magnesium. The coordinates of DDG were kindly provided by Tina Izard (Izard & Blackwell, 2000).

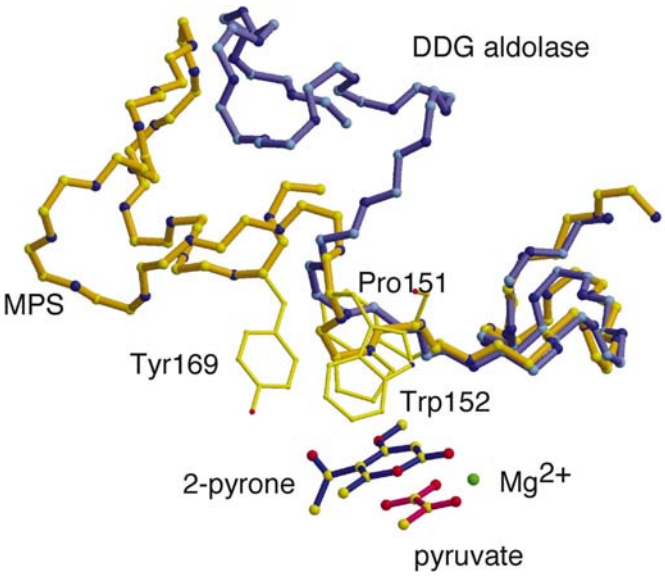

Figure 8
Superposition of the loops which cover the active site of MPS (yellow) and DDG aldolase (light blue). The hydrophobic and bulky side chains that interact with the substrate (2-pyrone) are indicated. The two substrates and the magnesium ion are also shown.

carbon of the aldehyde (Fish & Blumenthal, 1966) to accomplish condensation (Fig. 1*b*). Based on the crystal structure of DDG aldolase, it was proposed that the phosphate ion that is hydrogen bonded to the arginine side chain plays a role in abstracting the α-proton from pyruvate to form pyruvate enolate (Izard & Blackwell, 2000). MPS does not require such a molecule as a base and no adequate base is present at the active site of MPS to abstract a proton from the pyruvate. This finding supports the previous observation that pyruvate is a poor substrate in the reaction of MPS (Watanabe, Mie *et al.*, 2000). This finding is also consistent with our previous result that protonation of the enolate from solvent and the resultant formation of pyruvate are inhibited competitively by the 2-pyrone (2). The structure of the active site shows enough space for the binding of (2) below the enolate, whose binding limits the access of the solvent (Fig. 7).

The intermolecular Diels–Alder reaction between the enolate and the 2-pyrone (2) occurs in the second step of the MPS reaction (Figs. 1*a*, 6 and 7*a*). As mentioned above, steric congestion of the peptide backbone allows 2-pyrone access from only one side of the enolate plane, where the catalytic pocket is open. Figs. 6 and 7(*a*) show the proposed model for the very early transition state of the Diels–Alder reaction. In this binding model, two planes (2-pyrone and pyruvate enolate) are placed in parallel at a π-orbital overlapping distance. Several features are worth noticing in this model. Firstly, there are two side chains that have the ability to make hydrogen bonds to the 2-pyrone molecule. These hydrogen bonds are between the carbonyl O atom of 2-pyrone and Arg101, and between the C5 acyl O atom and Tyr169 (Fig. 6). The effect of these hydrogen bonds on the Diels–Alder reaction has been described previously (Ose *et al.*, 2003). Tyr169 is on the flexible loop from the threefold-related neighbouring protomer (Fig. 5). The stacking direction of 2-pyrone to pyruvate enolate is exactly that expected from the product.

DDG aldolase has structural features that allow low substrate specificity, *i.e.* the ability to condense a wide range of aldehydes with pyruvate (Fish & Blumenthal, 1966). Behind the active site of DDG aldolase, there is an open cavity along the direction of the product (galactarate) carbon skeleton (Fig. 7*b*). Izard and coworkers built the model of DDG aldolase complexed with DDG (Izard & Blackwell, 2000) (Fig. 7*b*). Compared with MPS modelled with 2-pyrone, the C4 position of DDG nearly corresponds to the C6 position of 2-pyrone. Therefore, the new carbon–carbon bonds of both enzymes are made at a relatively similar position (carbon–carbon bonding in MPS is one of the bonds formed by the Diels–Alder reaction) in both the active sites. The molecular skeleton from C3 to C5 of DDG also corresponds to the oxalacetate model incorporated in the model of MPS. This shows that DDG aldolase might chelate the oxalacetate and facilitate the production of pyruvate enolate.

The major differences between the substrates of the two enzymes, 2-pyrone and DDG, are in the hydrophobicity of the side chain as well as in its shape. Around the active site, there are hydrophobic and bulky residues such as Pro151, Trp152 and Trp278 that are characteristic of MPS (Fig. 8). The corresponding residues of DDG aldolase are Val125, Ser126 and Gly241, respectively. In particular, Pro151 seems to

interact directly with the pyrone ring in MPS. On the other hand, Leu216 is characteristic of DDG aldolase. The interaction between the residues and modelled DDG has been described previously (Izard & Blackwell, 2000) (Fig. 7*b*).

In an earlier paper, we reported the effect of the substituents of 2-pyrone on the enzymatic activity of MPS to catalyse its conversion to the corresponding benzoate (Watanabe, Mie *et al.*, 2000*c*). As shown in Fig. 7(*a*), there is sufficient space around the C4, C5 and C6 positions in our binding model. Basically, the spare space around the substrate of the two enzymes extends in the same direction. The hydrophobic nature of Leu216 seems to be important for recognizing the hydrophobic part around C4, C5 and C6 of DDG. The corresponding residue in MPS is Gly253. In this area in the active site of MPS, there is a large space around the C6 position of 2-pyrone, so that rather large substituents such as a phenyl group as well as a methyl group or H atom are also permitted in the substrate (Oikawa *et al.*, 2000; Watanabe, Mie *et al.*, 2000*c*) (Fig. 6). In our space-filling model of the active site (Fig. 7*a*), Tyr169 on the flexible loop moves into the proximity of the C5 acyl O atom of 2-pyrone substrates. The inserted loop from the neighbouring threefold-related protomer is composed of residues 140–170 in MPS and of residues 114–138 in DDG aldolase. The superimposition of these loop regions of both enzymes is shown in Fig. 8. The loop of MPS is longer than that of DDG aldolase by six residues. A short α-helix consisting of six residues (128–133) is assigned in this loop of DDG aldolase. The former half (residues 140–150 in MPS) of the loop can be superimposed; however, the latter half is inherently different. The region that corresponds to the area around Tyr169 in MPS is deleted in DDG aldolase.

The final chemical step of the enzymatic reaction of MPS is the elimination of water and carbon dioxide (Fig. 6). We have already explained that this is the rate-determining step and that the aberrant adduct formation from the reaction with 2-pyrone lacking the C4 methoxy group (Watanabe, Mie *et al.*, 2000*a*,*b*) led to our binding model. The stereochemical course of the conversion from the adduct (5) to macrophomate (1) is shown in Fig. 6. A stepwise mechanism for the degradation of (5) is eliminated for the following reasons. (i) The dehydration formally proceeds through *anti* elimination based on our observations (Watanabe, Mie *et al.*, 2000*a*). The rigid conformation of (5) prevents a suitable antiperiplanar conformation involving pro-*R* hydrogen at the C6 and C1 hydroxy group for E2 elimination. (ii) Formation of the unstable carbocation at C1 adjacent to the carboxylate (E1 elimination) is also less likely to take place. (iii) Decarboxylation and the subsequent dehydration require that the active site accepts a structurally distinct intermediate diene and catalyzes further dehydration. Thus, deprotonation concomitant with decarboxylation and elimination of the hydroxy group is the most probable route. In this route, the pro-*R* proton at C6 is located antiperiplanar to the cleaving C5—O bond. Since inspection of the active site does not identify any basic residues proximal to the pro-*R* proton, the C1 carboxylate may abstract the proton, with help from Arg101 in accepting the developing charge on the lactone O atom. The final elimination of the hydroxyl group would facilitate protonation by water, which may be further relayed to Ser148 and His73 (Fig. 6).

Enzymes containing $(\beta/\alpha)_8$-barrel (TIM-barrel) folds form the largest family of protein folds, with a wide range of functions. The $(\beta/\alpha)_8$-barrel fold protein is one of the most suitable examples for evaluating protein evolution based on protein structure. In this study, we compared two enzyme structures complexed with substrate to evaluate the structure–function relationship of $(\beta/\alpha)_8$-barrel fold proteins. Both MPS and DDG aldolase are classified as belonging to the 'enolase superfamily' based on their reaction strategy. The members of the enolase superfamily possess the ability to catalyze the abstraction of the α-proton of a carboxylate to form an enolate intermediate. The intermediates are induced to form the product by a specific active site in each enzyme; their reactions are diverse, including racemization, β-elimination of water, β-elimination of ammonia and cycloisomerization.

In the reaction of DDG aldolase, the enolization of pyruvate occurs and this enzyme-bound enolate then attacks the polarized C atom of the aldehyde to accomplish the condensation. In the MPS reaction, however, the pyruvate enolate is used as a dienophile for a Diels–Alder reaction. MPS takes advantage of forming pyruvate enolate from oxalacetate by adopting the strategy of oxalacetate decarboxylation. The Diels–Alder reaction does not basically require any catalytic processes by an enzyme. There have been three examples proposed as natural Diels–Alderases: solanapyrone synthase (Katayama *et al.*, 1998; Oikawa *et al.*, 1995; Oikawa *et al.*, 1998), lovastatin nonaketide synthase (Auclair *et al.*, 2000; Kennedy *et al.*, 1999) and MPS. These enzymes are not only Diels–Alderases but also catalyze oxidation, polyketide chain formation and decarboxylation prior to the Diels–Alder reaction, respectively. Here, we can see the advantage of natural enzymes compared with artificial catalytic antibodies; the products of the first reaction catalyzed by these enzymes are trapped in an active site, overlapping π-orbitals with another moiety for a [4 + 2] reaction and forming two new carbon–carbon bonds. The basic principles for carbon–carbon bond formation used in both MPS and DDG aldolase are the same with regard to trapping an enolate substrate and inducing subsequent reactions between two substrates. The difference is that one is a Diels–Alder reaction and the other is an aldol condensation. It seems that MPS allows the large structural change of the substrate/product during the Diels–Alder reaction. Changing the shape of the initial Diels–Alder reaction product is essential for escaping product inhibition. The optimized hydrophobic cavity of this enzyme makes this reaction possible.

We thank S. Wakatsuki, M. Suzuki and N. Igarashi of the Photon Factory, Japan for their kind help in data collection at beamline BL18B. We also thank T. Izard of St Jude Children's Research Hospital for kindly providing the coordinates of DDG and the DDG aldolase modelled structure. This work was supported in part by National Project on Protein Struc-

tural and Functional Analyses from the Ministry of Education, Science, Sports and Culture of Japan.

References

Abrahams, J. P. & Leslie, A. G. W. (1996). *Acta Cryst.* D**52**, 30–42.

Altschul, S. F., Gish, W., Miller, W., Myers, E. W. & Lipman, D. J. (1990). *J. Mol. Biol.* **215**, 403–410.

Auclair, K., Sutherland, A., Kennedy, J., Witter, D. J., Van den Heever, J. P., Hutchinson, C. R. & Vederas, J. C. (2000). *J. Am. Chem. Soc.* **122**, 11519–11520.

Bender, S. L., Widlanski, T. & Knowles, J. R. (1989). *Biochemistry*, **28**, 7560–7572.

Benziman, M., Russo, A., Hochman, S. & Weinhouse, H. (1978). *J. Bacteriol.* **134**, 1–9.

Braisted, A. C. & Schultz, P. G. (1991). *J. Am. Chem. Soc.* **112**, 7430–7431.

Brünger, A. T., Adams, P. D., Clore, G. M., DeLano, W. L., Gros, P., Grosse-Kunstleve, R. W., Jiang, J.-S., Kuszewski, J., Nilges, M., Pannu, N. S., Read, R. J., Rice, L. M., Simonson, T. & Warren, G. L. (1998). *Acta Cryst.* D**54**, 905–921.

Collaborative Computational Project, Number 4 (1994). *Acta Cryst.* D**50**, 760–763.

Fish, D. C. & Blumenthal, H. J. (1966). *Methods Enzymol.* **9**, 529–534.

Frauendorf, C. & Jäschke, A. (1998). *Angew. Chem. Int. Ed. Engl.* **37**, 1378–1381.

Gerlt, J. A. & Babbitt, P. C. (1998). *Curr. Opin. Chem. Biol.* **2**, 607–612.

Gouverneur, V. E., Houk, K. N., de Pascual-Teresa, B., Beno, B., Janda, K. D. & Lerner, R. A. (1993). *Science*, **262**, 204–208.

Heine, A., Stura, E. A., Yli-Kauhaluoma, J. T., Gao, C., Deng, Q., Beno, B. R., Houk, K. N., Janda, K. D. & Wilson, I. A. (1998). *Science*, **179**, 1934–1940.

Hilvert, D., Hill, K. W., Nared, K. D. & Auditor, M.-T. (1989). *J. Am. Chem. Soc.* **111**, 9261–9262.

Holm, L. & Sander, C. (1993). *J. Mol. Biol.* **233**, 123–138.

Huang, K., Li, Z., Jia, Y., Dunaway-Mariano, D. & Herzberg, O. (1999). *Structure*, **7**, 539–548.

Ichihara, A. & Oikawa, H. (1998). *Curr. Org. Chem.* **2**, 365–394.

Ichihara, A. & Oikawa, H. (1999). *Comprehensive Natural Products Chemistry*, Vol. 1, edited by D. Barton, K. Nakanishi & O. Meth-Cohn, pp. 367–408. Amsterdam: Elsevier.

Izard, T. & Blackwell, N. C. (2000). *EMBO J.* **19**, 3849–3856.

Jones, T. A., Zou, J. Y., Cowan, S. W. & Kjeldgaard, M. (1991). *Acta Cryst.* A**47**, 110–119.

Katayama, K., Kobayashi, T., Oikawa, H., Honma, M. & Ichihara, A. (1998). *Biochim. Biophys. Acta*, **1384**, 387–395.

Kennedy, J., Auclair, K., Kendrew, S. G., Park, C., Vederas, J. C. & Hutchinson, C. R. (1999). *Science*, **284**, 1368–1372.

Kleywegt, G. J. & Jones, T. A. (1998). *Acta Cryst.* D**54**, 1119–1131.

La Fortelle, E. de & Bricogne, G. (1997). *Methods Enzymol.* **276**, 472–294.

Laskowski, R. A., MacArthur, M. W., Moss, D. S. & Thornton, J. M. (1993). *J. Appl. Cryst.* **26**, 283–291.

Leslie, A. G. W. (1993). *Jnt CCP4/ESF–EACMB Newsl. Protein Crystallogr.* **26**, 27–33.

Matthews, B. W. (1968). *J. Mol. Biol.* **33**, 491–497.

Murzin, A. G., Brenner, S. E., Hubbard, T. & Chothia, C. (1995). *J. Mol. Biol.* **247**, 536–540.

Navaza, J. (1994). *Acta Cryst.* A**50**, 157–163.

Oikawa, H., Katayama, K., Suzuki, Y. & Ichihara, A. (1995). *J. Chem. Soc. Chem. Commun.* pp. 1321–1322.

Oikawa, H., Kobayashi, T., Katayama, K., Suzuki, Y. & Ichihara, A. (1998). *J. Org. Chem.* **63**, 8748–8756.

Oikawa, H., Watanabe, K., Yagi, K., Ohashi, S., Mie, T., Ichihara, A. & Honma, M. (1999). *Tetrahedron Lett.* **40**, 6983–6986.

Oikawa, H., Yagi, K., Ohashi, S., Watanabe, K., Mie, T., Ichihara, A., Honma, M. & Kobayashi, K. (2000). *Biosci. Biotechnol. Biochem.* **64**, 2368–2379.

Ose, T., Watanabe, K., Mie, T., Honma, M., Watanabe, H., Yao, M., Oikawa, H. & Tanaka, I. (2003). *Nature (London)*, **422**, 185–189.

Piccirilli, J. A., Rozzell, J. J. D. & Benner, S. A. (1987). *J. Am. Chem. Soc.* **109**, 8084–8085.

Romesberg, F. E., Spiller, B., Schultz, P. G. & Stevens, R. C. (1998). *Science*, **279**, 1929–1933.

Steinberger, R. & Westheimer, F. H. (1949). *J. Am. Chem. Soc*, **71**, 4158–4158.

Terwilliger, T. C. & Berendzen, J. (1999). *Acta Cryst.* D**55**, 849–861.

Waldrop, G. L., Braxton, B. F., Urbauer, J. L., Cleland, W. W. & Kiick, D. M. (1994). *Biochemistry*, **33**, 5262–5267.

Watanabe, K., Mie, T., Ichihara, A., Oikawa, H. & Honma, M. (2000*a*). *J. Biol. Chem.* **275**, 38393–38401.

Watanabe, K., Mie, T., Ichihara, A., Oikawa, H. & Honma, M. (2000*b*). *Tetrahedron Lett.* **41**, 1443–1446.

Watanabe, K., Mie, T., Ichihara, A., Oikawa, H. & Honma, M. (2000*c*). *Biosci. Biotechnol. Biochem.* **64**, 530–538.

Watanabe, K., Oikawa, H., Yagi, K., Ohashi, S., Mie, T., Ichihara, A. & Honma, M. (2000). *J. Biochem.* **127**, 467–473.

Xu, J., Deng, Q., Chen, J., Houk, K. N., Bartek, J., Hilvert, D. & Wilson, I. A. (1999). *Science*, **286**, 2345–2348.

Ylikauhaluoma, J. T., Ashley, J. A., Lo, C. H., Tucker, L., Wolfe, M. M. & Janda, K. D. (1995). *J. Am. Chem. Soc.* **117**, 7041–7047.